Table 2 Comparison of mode shapes, coupled flapwise, bending and torsion, fixed-free

I Mode

	IM, 11		TM	
$\bar{x}$	w	ϕ	w	ϕ
0.0	0.0000	0.0000	0.0000	0.0000
0.2	0.0639	0.0081	0.0639	0.0014
0.4	0.2299	0.0159	0.2299	0.0026
0.6	0.4611	0.0227	0.4611	0.0038
0.8	0.7255	0.0276	0.7255	0.0046
1.0	1.0000	0.0295	1.0000	0.0049

II Mode

	IM, 11		TM	
$\bar{x}$	w	ϕ	w	ϕ
0.00	0.0000	0.0000	0.0000	0.0000
0.2	−0.2952	−0.2020	−0.2950	−0.0337
0.4	−0.6681	−0.3499	−0.6678	−0.0583
0.6	−0.5712	−0.3874	−0.5710	−0.0646
0.8	0.0817	−0.3299	0.0817	−0.0550
1.0	1.0000	−0.2791	1.0000	−0.0465

III Mode

	IM, 11		TM	
$\bar{x}$	w	ϕ	w	ϕ
0.0	0.0000	0.0000	0.0000	0.0000
0.2	−0.0060	0.3093	−0.0361	0.3093
0.4	−0.0207	0.5860	−0.1242	0.5860
0.6	−0.0324	0.8057	−0.1946	0.8057
0.8	−0.0327	0.9493	−0.1962	0.9493
1.0	−0.0257	1.0000	−0.1541	1.0000

mode. In the above computations the integrating matrix corresponding to third-order polynomial and differentiating matrix corresponding to fourth-order polynomial are used. The integrating matrix is derived in Ref. 1 and the differentiating matrix can be obtained from the formulae given in Ref. 4. It can be seen from Table 2 that I and II are predominantly bending modes and III is predominantly a torsional mode. It is evident from this table that bending deflections are accurate for predominantly bending modes and torsional deflections are accurate for predominantly, torsional modes. Therefore the integrating and differentiating matrix method does not yield accurate deflections for non-predominant degrees of freedom in a coupled mode shape, the reason being that this approach yields a non-self-adjoint eigenvalue problem even though the original system is self-adjoint. This can be observed from the eigenvalue problem given by Eq. (8), that neither $[A]$ nor $[B]$ are symmetric matrices; consequently, the modal vectors defined by the eigenvalue problem are not orthogonal in the normal sense. To solve for the eigenvalues, the QR-transformation method (Ref. 5) is preferable rather than the conventional sweeping and iteration technique since the modal vectors are not orthogonal in the normal sense. Even though the original continuous system has orthogonality properties for its eigenfunctions, they cannot be used to solve Eq. (8), since any approximate formulation must be self-contained. But one could use biorthogonality relationships, which involve solutions of two eigenvalues problems: (a) the original eigenvalue problem, and (b) the adjoint eigenvalue problem. Since the present eigenvalue problem is non-self-adjoint, it is preferable to use the complex QR-transformation to look for the possibility of complex eigenvalues. However, such values are not encountered in the present computation, which is also similar to problem discussed in Ref. 1.

The present method breaks down when applied to a system containing rigid-body degrees of freedom. To illustrate this problem, the method is applied to a uniform continuous beam which is hinged at one end and free at the other end. The equation of motion for simple harmonic free vibration with frequency ω is given by

$$w'''' - \lambda w = 0$$

where

$$\lambda = m\omega^2/EI$$

Integrating this four times successfully yields the following equation:

$$\{w\} - \lambda[I]^4\{w\} + [I]^3\{k_1\} + [I]^2\{k_2\} + [I]\{k_3\} + \{k_4\} = \{0\}$$

By applying the boundary conditions ($w_0 = w_0'' = w_n'' = w_n''' = 0$) to determine the constants of integration $\{k_1\}$ $\{k_2\}$ $\{k_3\}$ and $\{k_4\}$ one can observe that $\{k_3\}$ will be left undetermined and $\{k_2\}$ will have two different values. The reason for the failure of this technique for semidefinite systems may be that this approach is leading to a flexibility type of formulation (in the sense that the eigenvalue $\lambda = 1/\omega^2$) and such a formulation cannot exist for a semidefinite system.

In spite of the failure of this technique to semidefinite systems and inaccurate non-predominant modes in coupled problems, the method is highly appealing because of the advantages discussed in Ref. 1.

References

[1]Hunter, W. F, "The Integrating Matrix Metod for Determining the Natural Vibration Characteristics of Propeller Blades," NASA TN D-6064, Dec. 1970.

[2]Hubolt, J. C. and Brooks, G. W., "Differential Equations of Motion for Combined Flapwise Bending, Chordwise Bending, and Torsion of Twisted Non-uniform Rotor Blades," NACA Report 1346, 1958.

[3]Murthy, V. R., "Determination of Structural Dynamic Characteristics of Rotor Blades and the Effect of Phase Angle on Multibladed Rotor Flutter," Ph.D. Dissertation, Aerospace Engineering Dept., Georgia Institute of Technology, Atlanta, Ga., 1974.

[4]Abramowitz, M. and Segun, I. A., *Handbook of Mathematical Functions*, Dover Publications, Inc., New York, 1965.

[5]Francis, J. G. F., "The QR-Transformation: A Unitary Analogue to the LR-Transformation," *Computer Journal*, Vol. 4, 1961, pp. 265-271.

Consistent Integral Thickness Utilization for Boundary Layers with Transverse Curvature

G.J. Hokenson*
STD Research Corporation, Arcadia, Calif.

Nomenclature

A = area
a = coefficient in Eqs. (16), $\bar{T}_w$
b = coefficient in Eqs. (16), $(\bar{T}_{aw} - \bar{T}_w)\epsilon$
c = coefficient in Eqs. (16), $1.0 - \bar{T}_{aw}$
C_f = skin friction coefficient

Received Sept. 16, 1976; revision received Dec. 16, 1976.
Index category: Boundary Layers and Convective Heat Transfer – Turbulent.

*Senior Scientist and Group Manager, Physical Sciences. Member AIAA.

D = local body diameter
H = shape factor, δ^*/θ
h = enthalpy
M = Mach number
N = exponent in power law property profiles
Pr = Prandtl number
R = local body radius
Re = Reynolds number
T = temperature
u = streamwise velocity component
W = two-dimensional width, Eq. (3)
x = streamwise coordinate
y = coordinate normal to body surface
α = local slope of body surface, Eq. (7)
γ = ratio of specific heats
δ = boundary-layer thickness
δ^* = displacement thickness, Eq. (1)
δ_h = enthalpy thickness
ϵ = function of Prandtl number and flowfield parameters
ρ = density
θ = momentum thickness, Eq. (2)
τ = transverse curvature parameter, Eq. (10)
η = normalized y coordinate, y/δ
$-$ = indicates quantities nondimensionalized by δ for integral thicknesses and by freestream values for dependent variables

Subscripts

aw = adiabatic wall conditions
∞ = freestream conditions
o = integral parameters in the form of Eqs. (11) and (12)
$2D$ = two dimensional
w = wall conditions

BOUNDARY-layer displacement and momentum thicknesses may be introduced by conceptually uniformizing the flowfield properties throughout the boundary layer. In order that the mass flux past the wall in the streamwise direction equal that in the boundary layer with nonuniform flow, the wall (and therefore the external flow streamlines) must be shifted a distance δ^* normal to its own plane. Expressed in mathematical terms, this can be written

$$\int_w^\infty \rho u \mathrm{d}A = \int_{\delta^*}^\infty \rho_\infty u_\infty \mathrm{d}A \tag{1}$$

Similarly, the net momentum defect of the nonuniform flow in the boundary layer must be matched by the uniformized flow, forcing the total momentum in a layer of thickness θ adjacent to the wall to be accounted for through the relationship

$$\int_w^\theta \rho_\infty u_\infty^2 \mathrm{d}A = \int_w^\infty \rho u(u_\infty - u)\mathrm{d}A \tag{2}$$

In both Eqs. (1) and (2) a coordinate system which is attached to the wall has been utilized and the y-axis is assumed to be normal to the local body surface. In the two-dimensional configuration, the differential area through the boundary layer is

$$\mathrm{d}A = W\mathrm{d}y \tag{3}$$

where W is the local transverse flowfield dimension. With this expression applied to Eqs. (1) and (2), the following classical formulas can be derived

$$\bar{\delta}^*_{2D} = \int_0^1 (1-\bar{\rho}\bar{u})\,\mathrm{d}\eta \tag{4}$$

and

$$\bar{\theta}_{2D} = \int_0^1 \bar{\rho}\bar{u}(1-\bar{u})\,\mathrm{d}\eta \tag{5}$$

The terms on the right hand side of Eqs. (4) and (5) are also the exact form of the grouping of variables which appear in the two-dimensional integral boundary-layer equations.

For the axisymmetric situation, the local differential area through the boundary layer may be written

$$\mathrm{d}A = 2\pi(R \pm y\cos\alpha)\mathrm{d}y \tag{6}$$

where:

$$\alpha \equiv \tan^{-1}(\mathrm{d}R/\mathrm{d}x) \tag{7}$$

The + or − sign in Eq. (6) is applicable to external or internal flows respectively and R is the local perpendicular distance from the axis of symmetry to the body surface. Utilizing this differential area in Eqs. (1) and (2) results in the following expressions for the displacement and momentum thickness

$$\tau\bar{\delta}^{*2} + \bar{\delta}^* - \int_0^1 (1-\bar{\rho}\bar{u})\,(1+2\tau\eta)\,\mathrm{d}\eta = 0 \tag{8}$$

and:

$$\tau\bar{\theta}^2 + \bar{\theta} - \int_0^1 \bar{\rho}\bar{u}(1-\bar{u})\,(1+2\tau\eta)\,\mathrm{d}\eta = 0 \tag{9}$$

Two-dimensional flows are embedded in this general formulation as the limiting case of $\tau = 0$, where

$$\tau \equiv \pm\delta\cos\alpha/D \tag{10}$$

and the $\pm$ sign carries the same significance as previously noted. Since τ, $\bar{\delta}^*$ and $\bar{\theta}$ are significantly less than unity for the majority of cases of interest, Eqs. (8) and (9) can generally be approximated by

$$\bar{\delta}^*_o = \int_0^1 (1-\bar{\rho}\bar{u})\,(1+2\tau\eta)\,\mathrm{d}\eta \tag{11}$$

and

$$\bar{\theta}_o = \int_0^1 \bar{\rho}\bar{u}(1-\bar{u})\,(1+2\tau\eta)\mathrm{d}\eta \tag{12}$$

Upon integrating the axisymmetric equations of motion across the boundary layer (Ref. 1), the resulting momentum integral equation explicitly involves the terms H_o and θ_o in the form

$$\frac{\mathrm{d}\theta_o}{\mathrm{d}x} + \theta_o\left\{\frac{\mathrm{d}\ell n u_\infty}{\mathrm{d}x}\,[H_o + 2 - M_\infty^2] + \frac{\mathrm{d}\ell n D}{\mathrm{d}x}\right\} = \frac{C_f}{2} \tag{13}$$

where

$$H \equiv \delta^*_o/\theta_o \tag{14}$$

and δ^*_o and θ_o (i.e. $\bar{\delta}^*_o\delta$ and $\bar{\theta}_o\delta$) are calculated from the dimensional counterparts of Eqs. (11) and (12).

It is now apparent that the uniformly valid physical descriptions of the displacement and momentum thickness, as expressed mathematically by Eqs. (1) and (2), supply relationships which are identical to those appearing in the governing momentum integral equations for values of τ generally encountered. However, for cases of large τ with flowfield conditions which generate large values of $\bar{\delta}^*$ and $\bar{\theta}$, Eqs. (8) and (9) should be applied when calculating the integral thickness parameters which have been described physically ($\bar{\delta}^*$, $\bar{\theta}$), while the appropriate forms of δ^*_o and θ_o are utilized in the solution of the equations of motion.

The principal point of this Note is to emphasize those situations in which the terms $\bar{\delta}^*$ and $\bar{\theta}$ are being considered,

apart from their relationship to terms appearing in the governing conservation equations, and in which the expressions generally employed for their evaluation are those appropriate to $\bar{\delta}^*_o$ and $\bar{\theta}_o$. For example, consistent empirical correlation of the skin friction coefficient with momentum thickness and the shape factor with the various independent flowfield parameters should extend more universally into the large τ domain utilizing the general expressions contained in Eqs. (8) and (9). In addition, the use of displacement thickness distributions to generate "effective bodies" in hypersonic flow utilizing the tangent cone approximation or in the study of the entry region of an axisymmetric pipe flow would benefit from the use of Eqs. (8) and (9) which result directly from the simple physical descriptions of displacement and momentum thicknesses.

The results of the investigation reported here provide general indications of the limits on τ for which the terms $\bar{\theta}_o$, $\bar{\delta}^*_o$ and H_o that arise from the integral conservation equations are valid measures of $\bar{\theta}$, $\bar{\delta}^*$ and H which have their basis in the development leading to Eqs. (1) and (2). Given the dependence of $\bar{\theta}$, $\bar{\delta}^*$ and H on τ and the parameters which characterize the flowfield, the values of $\bar{\theta}_o$, $\bar{\delta}^*_o$ and H_o can be obtained from the following relations, derivable from Eqs. (8), (9), (11), and (12):

$$\frac{\bar{\theta}_o - \bar{\theta}}{\bar{\theta}} = \tau\bar{\theta} \tag{15a}$$

$$\frac{\bar{\delta}^*_o - \bar{\delta}^*}{\bar{\delta}^*} = \tau\bar{\theta}H \tag{15b}$$

$$\frac{H_o - H}{H} = \frac{\tau\bar{\theta}}{1+\tau\bar{\theta}}(H-1) \tag{15c}$$

These equations also provide the percentage difference between the two sets of integral thickness variables of interest.

In order to determine the quantitative effect of τ on the displacement and momentum thicknesses for a representative case of interest, the following formulas for the distributions of velocity and temperature through a constant pressure turbulent boundary layer have been utilized:

$$\bar{u} = \eta^{1/N} \tag{16a}$$

$$\bar{T} = a + b\eta^{1/N} + c\eta^{2/N} \tag{16b}$$

For these computations, the term ϵ in the coefficient b of Eq. (16b), which characterizes the lack of similarity between the velocity and temperature fields for Prandtl numbers different from one, has been set equal to unity.

If it is assumed that the pressure is constant across the boundary layer (another aspect of large τ layers to be quantitatively evaluated), Eqs. (16) can be applied to Eqs. (8) and (9) and the resultant integral parameters computed as a function of the principal independent flowfield variables

$$\bar{\theta}, \bar{\delta}^*, H = \bar{\theta}, \bar{\delta}^*, H(\gamma, Pr, \bar{T}_w, M_\infty N, \tau) \tag{17}$$

The effects of γ, Pr, M_∞ and N did not significantly affect the specification of a characteristic τ for which the integral boundary-layer characteristics, as evaluated by Eqs. (8) and (9), depart from the values calculated from Eqs. (11) and (12). Therefore, at $M_\infty = 2$ and $N = 7$, the influence of $\bar{T}_w$ and τ on the integral parameters $\bar{\theta}$ and H has been computed for air with $\gamma = 1.4$ and $Pr = .72$ as shown in Fig. 1. The data encompass a wide range of values for τ and $\bar{T}_w$, not because they are physically likely to occur but solely to expose the variable dependences of interest.

Mach numbers from 0→4 and power-law exponents from 5→10 all exhibited curves of similar shape. At higher Mach numbers the sensitivity of H to τ for cold wall conditions

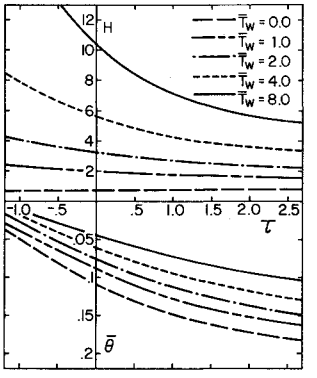

Fig. 1 Dependence of $\bar{\theta}$ and H on τ and T_w for a constant pressure turbulent boundary layer. $M_\infty = 2$, $N = 7$, $\gamma = 1.4$ and $Pr = 0.72$.

becomes increasingly positive while the shift in position of the curves for a varying N amounted to a few percent for each integer change in the exponent.

Utilizing the results presented in Fig. 1 and Eqs. (15), the percentage difference between the two displacement thicknesses at $\tau = 1.0$ and $\bar{T}_w = 4.0$ has been calculated to be 40% while the shape factors differ by 28%. It is thus clear that, for high τ boundary layers, utilization of the physically describable entities $\bar{\delta}^*$ and $\bar{\theta}$ must be carefully distinguished from the terms $\bar{\delta}^*_o$ and $\bar{\theta}_o$ which arise in the governing integral conservation equations.

To this point, other commonly used integral boundary-layer thicknesses (Ref. 3) have been neglected, inasmuch as their usefulness lies primarily in the fact that they allow the governing equations to be presented in a compact formulation. Their application to procedures outside the scope of solving the equations is relatively limited. One infrequent exception is the use of the enthalpy thickness (δ_h) to correlate the dependence of the Stanton number on the Reynolds number, Re_{δ_h}, as shown in Ref. 2.

The enthalpy thickness can be introduced on a purely physical basis in a manner identical to that used for the momentum thickness. The resulting mathematical expression for this physical entity is

$$\tau\bar{\delta}_h^2 + \bar{\delta}_h - \int_0^1 \bar{\rho}\bar{u}(\bar{h}-1)(1+2\tau\eta)\mathrm{d}\eta = 0 \tag{18}$$

By integrating the axisymmetric energy equation through the boundary layer, the term $\bar{\delta}_{h_o}$ arises naturally from the integration procedure, where

$$\bar{\delta}_{h_o} \equiv \int_0^1 \bar{\rho}\bar{u}(\bar{h}-1)(1+2\tau\eta)\mathrm{d}\eta \tag{19}$$

Eq. (18) can therefore be written:

$$\tau\bar{\delta}_h^2 + \bar{\delta}_h - \bar{\delta}_{h_o} = 0 \tag{20}$$

However, for a perfect gas boundary-layer flow with constant pressure across the viscous region, it is possible to show that

$$\bar{\delta}_{h_o} = \bar{\delta}^*_o - \int_0^1 (1-\bar{u})(1+2\tau\eta)\mathrm{d}\eta \tag{21}$$

If a velocity profile of the form presented in Eqs. (16) is utilized, Eq. (21) results in

$$\bar{\delta}_{h_o} = \bar{\delta}^*_o - \left[\frac{N+(1+\tau)(N+1)}{(N+1)(2N+1)}\right] \tag{22}$$

Therefore, the generalized enthalpy thickness, with which the convective heat transfer is to be correlated, may be computed from Eq. (20), written in the form

$$\bar{\delta}_h = (-1+\sqrt{1+4\tau\bar{\delta}_{j_o}})/2\tau \tag{23}$$

with $\bar{\delta}_{h_0}$ being evaluated utilizing Eq. (22) and the results of computations similar to those presented in Fig. 1.

Finally, the generalized definitions for each of the integral thicknesses employed here are compatible with the limiting case of axial boundary-layer flow over a needle. In this situation τ approaches infinity and each of the integrals reduces to the form of the following equation for displacement thickness

$$\overline{\delta^*}_{\tau \gg 1} = \left(\int_0^1 (1 - \bar{\rho}\bar{u})\, d\eta^2 \right)^{1/2} \tag{24}$$

Acknowledgment

The author would like to acknowledge the very helpful critique provided by F.E.C. Culick.

References

[1]Scholkemeier, F.W., Die laminare Reibungsschicht an rottationssymmetrischen Körpern, *Archiv der Mathematik.*, Vol. 1, 1949, pp. 270-277.

[2]Kutateladze, S.S., Leont'ev, A.I., "Boundary Layers in Compressible Gases," translated by Spalding, D.B., Academic Press, New York, 1964.

[3]Schlichting, H., *Boundary Layer Theory*, 6th edition, McGraw-Hill, New York, 1968.

Effect of Crystallization Kinetics on Rocket Performance

Charles B. Henderson*

Atlantic Research Corporation, Alexandria, Va.

Nomenclature

A,n	= constants in crystallization velocity equation
C	= specific heat capacity per unit mass
d	= diameter
k	= thermal conductivity
M	= Mach number
(MW)	= molecular weight
P	= pressure
R	= universal gas law constant
Re	= Reynolds number
T	= temperature
V	= velocity of crystallization wave
γ	= ratio of specific heats
μ	= viscosity
ρ	= density

Subscripts

F	= fusion
g	= gas
M	= equilibrium melting
P	= particle
t	= throat

Introduction

THE performance at high expansion ratios of metal-containing solid rocket propellants is sensitive to the recovery of the latent heat of fusion of the metal oxides formed in the combustion products. The thermal radiation from the plumes of such rocket exhausts, as a consequence of its dependency on the temperature of the particulates, is also sensitive to the recovery of the latent heat of fusion. An extensive literature exists on the kinetics of nucleation and crystal growth in liquids. There has been very little application of this research, however, to the problems just described.

Received Nov. 22, 1976.

Index categories: Solid and Hybrid Rocket Engines; Fuels and Propellants, Properties of.

*Vice President. Associate Fellow AIAA.

Review of Crystallization Kinetics

Both homogeneous nucleation and heterogeneous nucleation play a role in the fusion of a liquid droplet in a temperature-decreasing gas stream. The fusion process starts by homogeneous nucleation, that is by the spontaneous formation of molecular aggregates in an otherwise homogeneous liquid. Once the crystallization process has been initiated, fusion can also proceed by the process of heterogeneous nucleation in which the nuclei are formed at the interface between the liquid and the already-formed crystal phase.

From homogeneous nucleation theory[1,2] it may be inferred that the nucleation frequency is such a strong function of the temperature that it is permissible to define a homogeneous fusion temperature, T_F, which is a function only of the equilibrium fusion temperature, T_M. Above T_F, nuclei form too slowly to be of practical importance. Below T_F, nuclei form at exceedingly high rates. This inference has been confirmed experimentally; T_F has been found to be approximately 0.8 T_M for a wide variety of materials.[2-5] If only homogeneous nucleation is considered in solidification problems, the liquid is assumed to fuse at the temperature T_F, just as if it were an equilibrium thermodynamic melting temperature. This oversimplified approach has been previously used[6] in the prediction of rocket performance.

If a liquid melt were at uniform temperature, only homogeneous nucleation need be considered; this is not the case, however, with a liquid droplet in a temperature-decreasing gas stream. Fusion commences when the temperature at the outside of the drop reaches T_F. At this point, as discussed below, the temperature of that portion of the drop undergoing fusion increases, and homogeneous nucleation ceases to be of importance. Once homogeneous nucleation has provided a crystal phase, crystallization proceeds in a wavelike manner throughout the remainder of the liquid phase by the process of heterogeneous nucleation. An equation giving the linear velocity of the interface was derived by Hillig and Turnbull,[7] who modify a Volmer-type rate expression by assuming that only a fraction of the total sites on the crystal surface are available for molecular attachment; the number of sites is based on an assumption that crystallization occurs via a screw-dislocation mechanism. In the resulting expression, the velocity of the crystallization wave is proportional to the square of the supercooling; i.e., $V = A(T_M - T)^n$ where $n = 2$. A number of experimental investigators[7,8] have found that n is usually somewhat less than 2, namely 1.7-1.8.

Application of the crystallization velocity equation to a liquid drop in a temperature-decreasing gas stream leads to a rationalization of the phenomenon of recalescence in which, once crystallization has begun, the surface temperature of the drop rises as a consequence of the liberation of latent energy of fusion. This has been often detected experimentally by a sudden increase in the luminosity of the particle giving rise to the designation of spearpoint temperature, T_{sp}, to the maximum temperature achieved by the solidifying droplet.

The constants A and n in the wave velocity expression have been measured for zirconium oxide by Rosner and Epstein[8] who gave values of 0.72×10^{-4} cm/sec/K$^{1.8}$ and 1.8, respectively. No data have been found for aluminum oxide, but the theory of Hillig and Turnbull[1] suggests that the rates for the two oxides should be of the same order of magnitude.

Results and Discussion

The kinetics of crystallization presented previously have been applied to the rocket propellant exhaust by making one-dimensional calculations of a two-phase, nonreacting nozzle